An Electrical Circuit for Performance Analysis of Polymer Electrolyte Fuel Cell Stacks Using Electrochemical Impedance Spectroscopy

Samuel Cruz-Manzo and Rui Chen*

Department of Aeronautical and Automotive Engineering, Loughborough University, LE11 3TU, UK

*R.Chen@lboro.ac.uk

Abstract

In this study, a new electrical circuit is developed to evaluate the performance of polymer electrolyte fuel cell (PEFC) stacks using electrochemical impedance spectroscopy (EIS). Experimental EIS measurements were carried out in an open-cathode PEFC stack to validate the new electrical circuit. The electrical circuit developed in the authors' previous study, which simulates the impedance response of a single PEFC, is applied to EIS measurements carried out in the open-cathode PEFC stack. However, it cannot reproduce EIS measurements with positive imaginary components at low frequencies. Thus, in this study, the electrical circuit is modified by adding electrical components which represent intermediate adsorbed species in a two-step electrochemical reaction as reported in the literature. The results show that the new electrical circuit can accurately reproduce the experimental EIS measurements and can give an insight into the factors that limit the performance of the PEFC stack. This new electrical circuit can enable an assessment of the state of health and performance of the fuel cell stacks.

Keywords: electrical circuit, PEFC stack, EIS, electrochemical mechanisms

1. Introduction

In responding to the invitation from the organiser of ABAF 13 Conference, this paper extends the results reported in the conference ECS transaction volume 48 focusing on the development of a new electric circuit to evaluate PEFC stack performances.

Polymer electrolyte fuel cells (PEFCs) generate electrical and thermal energy by combining hydrogen and oxygen. PEFC stacks have to survive under a range of operational environments varying from, for example, a winter low of sub-zero air temperatures to a summer high relative humidity. For instance, open-cathode PEFCs have to survive under a range of atmospheric compositions which can include sulphur dioxide, nitrogen oxides and ionic contamination, as well as fuel impurities that can all potentially cause irreversible damage to the PEFC [1]. The list of critical contaminants is much longer if we also consider the effects of battlefield gases for military applications [2]. Electrochemical impedance spectroscopy (EIS) is a powerful technique that can be applied in-situ for diagnosis of the PEFC performance. The resulting impedance is commonly shown in a complex plane and represents the electrochemical and diffusion mechanisms in the frequency domain. The use of equivalent electrical circuits with the experimental EIS technique is a well-established methodology to characterise processes in the PEFC. An electrical circuit can represent an identical impedance response to that obtained from the electrochemical studied. Each electrical component in the electrical circuit describes a physical process that takes place in the electrochemical system. In the authors' previous study [3] an electrical circuit was developed to simulate and characterise the frequency response of a single PEFC at any current of the polarisation curve. However, the electrical circuit had limitations in reproducing EIS measurements with positive imaginary components at low frequencies. EIS measurements with positive imaginary components at low frequencies are known as an inductive loop and have been reported in the impedance response of PEFCs stacks [4]. Makharia *et al.* [5] suggested that the possible reason for this inductive effect at low frequencies are the side reaction and intermediates involved in fuel cell reactions. Roy *et al.* [6] developed an impedance model to account for the reaction mechanisms that may be responsible for the inductive response at low frequencies, the model proposes the formation of hydrogen peroxide (H_2O_2) as an intermediate in a two-step oxygen

reduction reaction (ORR). It has been reported [7] that crossover of hydrogen to the cathode facilitates the reaction of oxygen and hydrogen at the cathode, generating hydroxyl and hydroperoxyl radicals which react further to produce H_2O_2 at the cathode. The hypothesis that H_2O_2 may be formed at the cathode of a fuel cell is supported by the results of Inaba *et al.* [8]. In this study, the electrical circuit reported in the author's previous study [3] and developed from simple reaction kinetics $Ox + e^- \overset{K}{\leftrightarrow} \mathrm{Re}$ is modified by including electrical components which represent intermediate species in a two-step ORR. The resulting electrical circuit is validated against the frequency response of an open-cathode 4-cell stack. This new electrical circuit can provide an insight into the mechanisms that limit the performance of PEFC stacks.

2. Experimental

A commercial open-cathode 4-cell stack with a 16 cm^2 area was used for the experimental tests. The membrane electrode assemblies (MEAs) were made of Nafion 211 with platinum loadings of 0.4mg/cm^2 and carbon black for the electrodes. The gas diffusion layers (GDLs) were made of carbon felt with 200 µm width. The 4-cell stack consists of open cathodes with two 5V DC fans for oxidant supply (as air) and cooling, as shown in Fig. 1a. The stack consists of bipolar plates made of FU4369 HT material with a thickness of 5 mm.

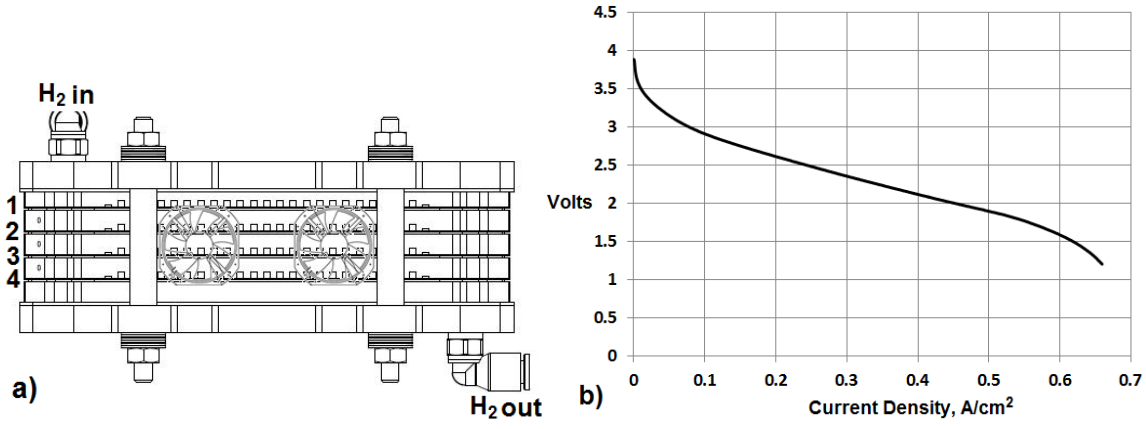

Figure 1. a) Open-cathode fuel cell stack for EIS measurements, 1b) Polarisation curve

High purity hydrogen (99.999 %) was used during the tests. The fuel cell stack was run in a through flow mode at the anode. Flow rate of hydrogen in the anode was kept constant during all the

experiments with a stoichiometry of 2. The hydrogen supplied was dry. The PEFC stack was operated at ambient temperature 22 °C and the hydrogen back pressure was held at 0.4 bar(g). Polarisation curves were recorded prior to impedance measurements, as shown in Fig. 1b.

EIS measurements were carried out through a multichannel frequency response analyzer FRA (Z#106 WonATech Co). The multichannel FRA consists of five channels and simultaneously measures five impedance spectra through a single induced DC current value. The multichannel system is connected with a RBL488 Dynaload. The EIS measurements were carried out in a galvanostatic mode with a 5% AC amplitude of the DC current to obtain a linear response from the system at frequencies from 10 kHz to 0.1Hz. Five channels from the Z#106 FRA were used to simultaneously measure the impedance of the PEFC stack and the impedance solely for each cell. EIS measurements were carried out at three different current densities 0.1875, 0.3125, and 0.4375 A/cm^2 of the polarisation curve shown in Fig. 1b. The PEFC stack was run over 60 minutes at the required current with no variation in the voltage to ensure a steady state for EIS measurements. EIS measurements for current densities < 0.1875 A/cm^2 were not possible, as the low AC amplitude superimposed onto the DC current made it difficult for the FRA to distinguish between noise and response. At high current densities >0.4365 A/cm^2 the stack was not steady for a long period of time due to the high water concentration produced by the oxygen reduction reaction (ORR).

Stack Measurements.- The resulting stack impedance is shown in a complex plane and represents the electrochemical and diffusion mechanisms in the frequency domain. The diameter of the spectrum decreases from a current density of 0.1875 A/cm^2 to 0.3125 A/cm^2 and increases from a current density of 0.3125 A/cm^2 to 0.4375 A/cm^2, as shown in Fig. 2.

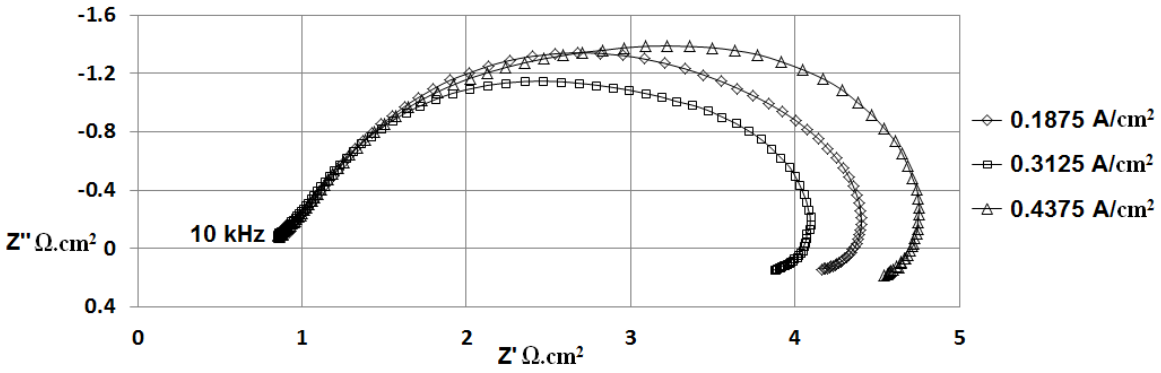

Figure 2. PEFC stack measured impedance data at 0.1875, 0.3125 and 0.4375 A/cm^2

In the authors' previous study [9] a reference electrode inserted in a PEFC operated with 100% relative humidity in the anode and a multichannel frequency response analyser allowed the separation of the impedance response of the cell and cathode. The results showed that anode mechanisms (hydrogen oxidation reaction) have not contribution in EIS measurements at medium and high currents. Springer *et al.* [10] reported that there is a negligible difference in impedance response when measuring the cathode impedance relative to the anode or relative to a reference electrode place on the side of the anode. In this study, it was not possible to insert reference electrodes in the open-cathode PEFC stack to measure the impedance response for each electrode. Therefore based on anode impedance results reported in the literature [9,10,11,12]; the anode contribution on these EIS measurements, neglecting any contaminant within the hydrogen supplied such as CO which affects the PEFC performance [13], will be considered negligible.

EIS measurements have limitations and present disadvantages as the low impedance values are obscured for low frequencies and some effects are not visible due to a masking effect in the impedance plot [14]. Therefore the impedance results of Fig. 2 reflect the overlapping of two semicircles. One at high-medium frequencies is related to the charge transfer resistance during the ORR and decreases with increasing current density, and the other at low frequencies is related to oxygen transport limitations and increases with increasing current density [9]. At high frequencies there is no inductive effect (EIS measurements with positive imaginary components Z'') of the measurement cables which deforms the high frequency region of the impedance spectra [15]. The

sensing cables of the FRA were directly connected to the bipolar plates of the PEFC stack. This allowed the reduction of inductive effects on the EIS measurements at high frequencies by placing the sensing cables from the FRA as far apart as possible from the inductive source (electric cables). At high frequencies, Fig. 2, it is clearly shown that the 45° straight line represents the ionic resistance of the catalyst layer as discussed in a previous study [15]. At low frequencies inductive effects on the EIS results were apparent for the three current densities. The literature [5,6,7,8] have suggested that the possible reason for this inductive effect at low frequencies are the side reaction and intermediates involved in fuel cell reactions.

Individual Cell Measurements. The use of the multichannel FRA allows the measurement of the impedance response of each cell of the PEFC stack simultaneously. The cells were numbered from the hydrogen inlet side starting from 1, as shown in Fig.1a. Fig. 3 shows the impedance response for the four cells at 0.1875 A/cm^2. The four cells show the inductive effect at low frequencies. There is little difference observed in this inductive effect at low frequencies for the cells at different positions in the stack. The cell located closer to the hydrogen inlet (cell 1) results in a smaller impedance spectrum than the other cells, as shown in Fig. 3. The second cell shows the biggest impedance spectrum which could be related to the structural features of the MEA. The measured data from 10 kHz to 100 Hz are similar for cells 1, 3 and 4. The difference in impedance response at low frequencies in cells 1, 3 and 4 could be related to limitations in oxygen transport through the cathode.

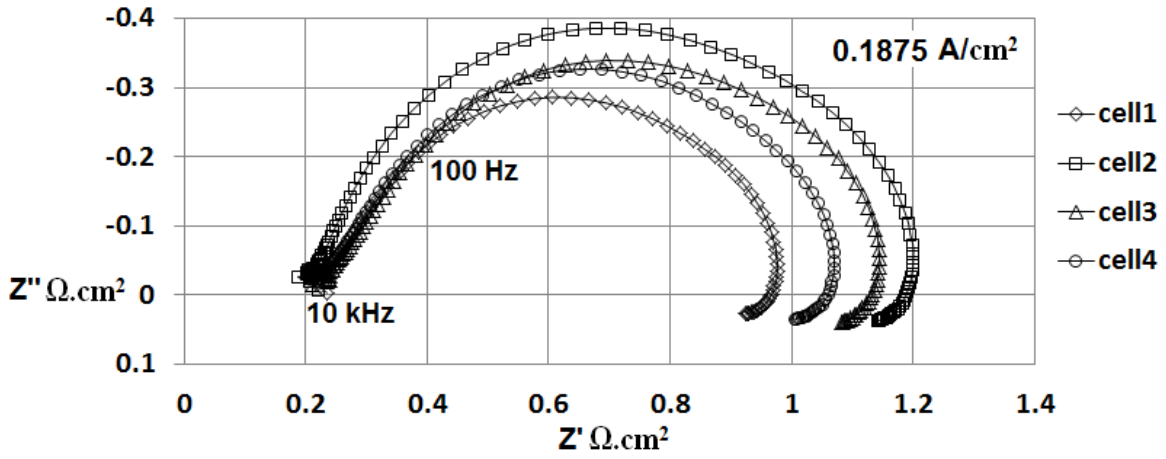

Figure 3. Measured impedance data for different cells of the stack at 0.1875 A/cm^2

Fig. 4 shows the impedance results of the four cells at a current density of 0.3125 A/cm^2. The diameters of the spectra decrease with increasing current density from 0.1875 A/cm^2 to 0.3125 A/cm^2. When the kinetics of the ORR dominate the cell performance such as in the low current density range of the polarisation curve, the impedance spectrum mainly represents the charge transfer resistance during the ORR and its diameter decreases with increasing current density [14]. At a current density of 0.3125 A/cm^2 there is an increase in the driving force for the interfacial oxygen reduction process. The impedance spectrum of cell 3 at low frequencies is bigger than cells 1 and 4. Cell 2 shows the biggest impedance spectrum.

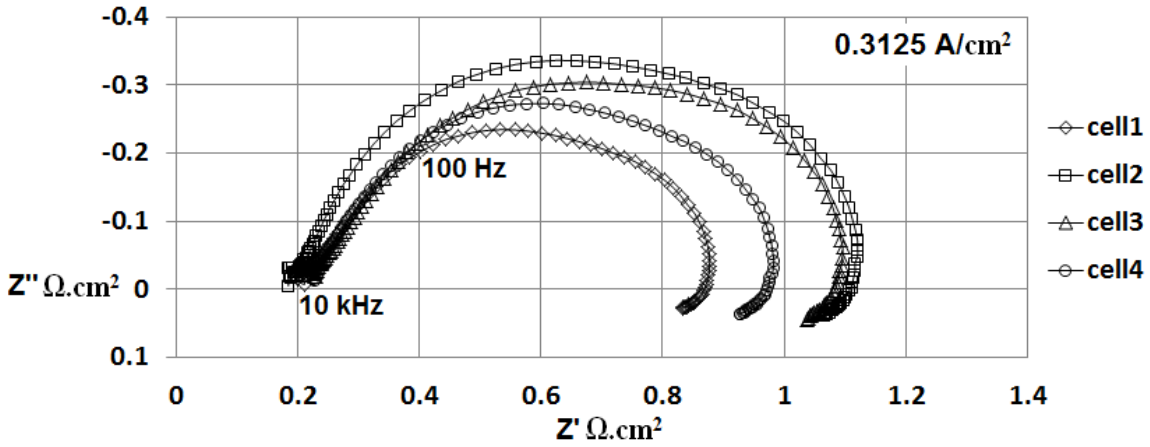

Figure 4. Measured impedance data for different cells of the stack at 0.3125 A/cm^2

Fig. 5 shows the impedance results at a current density of 0.4375 A/cm2. One of the disadvantages of the EIS technique is that multiple energy controlled processes during the electrochemical reaction can be masked in the impedance plot. Therefore in Fig. 5 the semicircles that represent the charge transfer of the ORR and mass transport effects are overlapped in the experimental impedance spectra. Similar results were reported by Yuan *et al.* [16] when EIS measurements were carried out in a H_2/air PEFC stack. Their results show that EIS measured data feature a single semicircle at high current densities. The increase in diameter of the spectra with increasing current density from 0.3125 A/cm^2 to 0.4375 A/cm^2 as shown in Fig. 5 is attributed to an increase in oxygen transport limitations [9].

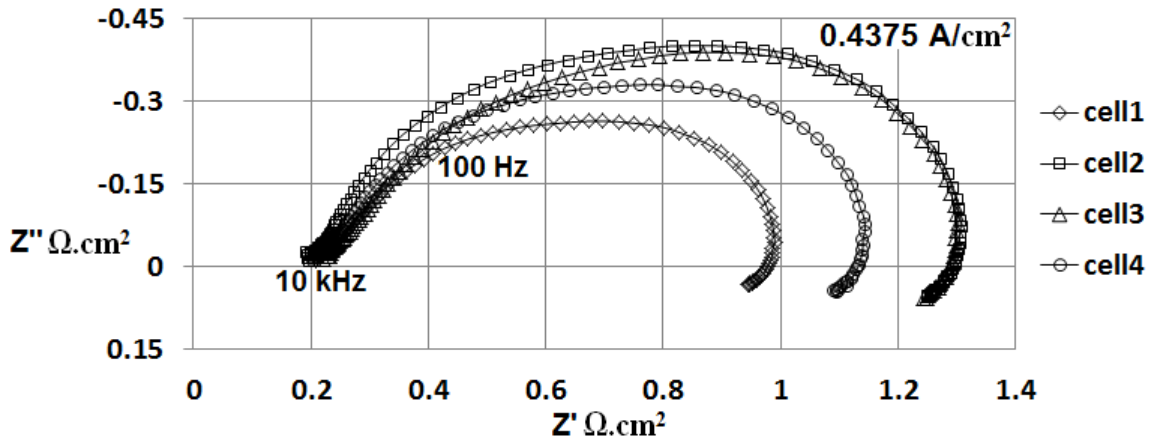

Figure 5. Measured impedance data for different cells of the stack at 0.4375 A/cm^2

3. Previous electrical circuit for EIS analysis

In the author's previous study [3] an electrical circuit was developed based on fundamental electrochemical theory to simulate the impedance response of the cathodic side of a PEFC at any current of the polarisation curve. The circuit consisted of a transmission line with distributed Warburg elements as shown in Fig. 6

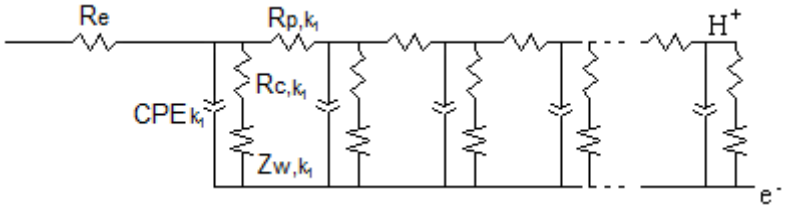

Figure 6. Previous electrical circuit for the PEFC characterisation (no anode contribution) [3]

The mathematical equation of the circuit shown in Fig. 6 is represented as:

$$Z_{FC} = R_e + \frac{(R_C + Z_W)\gamma \coth(\gamma x)}{1 + Y(i\omega)^P (R_C + Z_W)} \qquad [1]$$

with $\gamma = \sqrt{R_p \left[\frac{1}{R_C + Z_W} + Y(i\omega)^P \right]}$

where R_P is the resistance to the flow of ions in the electrolytic phase of the CCL; R_C represents the charge transfer resistance presented in the ORR and is defined as $R_C = b / j_0 \exp(\eta_S / b)$, where b is the Tafel slope, η_S represents a value of voltage in activation overpotential, and j_0 is the exchange current; $Z_W = R_W \tanh(i\omega T_W)^{0.5} / (i\omega T_W)^{0.5}$ is defined as the Warburg impedance and describes diffusion across a finite dimension in the frequency domain [17], with $R_W = RT\delta / (z^2 F^2 c_o^* D)$ defined as resistance for the diffusion process and $T_W = \delta^2 / D$ defined as the time constant to diffuse oxygen through the CCL; Y represents a parameter related to capacitance, superscript P represents a parameter to correct the inhomogeneity in the distribution of charge between the electrode-electrolyte inteface; ω is the angular frequency; i is the imaginary component in impedance; *Re* represents the total ohmic resistance to flow electrons and ions in the bipolar plate, GDL and PEM; x represents the thickness of the CCL (dimensionless) and for EIS measurements is equal to 1.

The simulated data from Eq. 1 were compared with the measured EIS data using a Graphic User Interface (GUI) developed in Matlab®. The use of the GUI with Eq. 1 for EIS analysis has already been demonstrated in the authors' previous study [3,9,15]. The GUI allows the fitting of the parameters from Eq. 1 to achieve a good agreement between the experimental and simulated data. In Eq. 1 there are some parameters that can also be estimated through a graphical interpretation of the Nyquist plot. This allows the reduction of the number of parameters to be fitted with the measured EIS spectra. R_e can be estimated through the high frequency limit of the real part Z', R_p can be estimated by projecting the 45^o straight line at the high frequency end of the spectrum and multiplying by three [5]. R_C can be calculated from the following relationships $C = Y / (R_e^{-1} + R_c^{-1})^{1-P}$ [18] and $C = Y(2\pi f_C)^{P-1}$ [19]; note that f_C is the characteristic frequency at which the negative imaginary part of the impedance reaches its minimum value, and the value of superscript P is between 0.8 and 0.85 as reported in literature [17,18]. The least squares fitting method was used in order to find the best-fit between the model and the measured data. A good quality fit is obtained when the sum of the deviations squared (least square error) between the simulated and measured impedance data has a

minimum value, for instance < 0.1. The results show that Eq. 1 cannot reproduce EIS measurements in the positive imaginary part of the complex impedance plane at low frequencies as shown in Fig. 7.

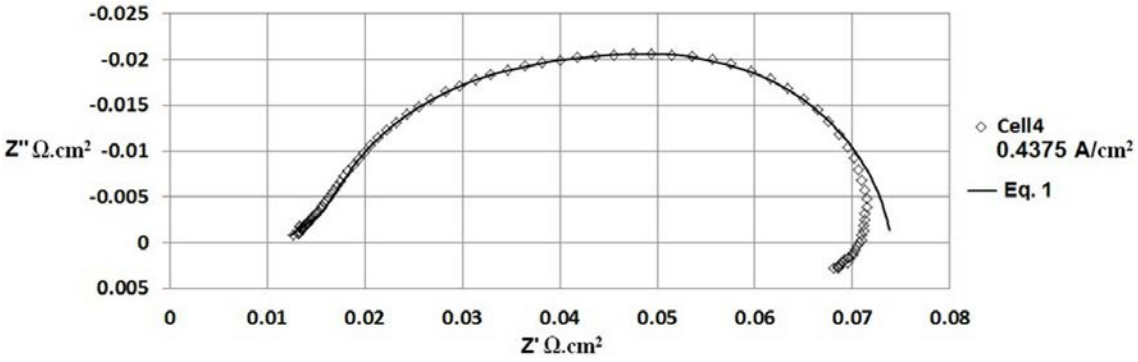

Figure 7. Comparison between measured data and simulated data from Eq. 1

4. New electrical circuit for PEFC stack analysis

The electrical circuit developed in a previous study [3] and shown in Fig. 6 cannot reproduce EIS measurements with positive imaginary components at low frequencies. EIS measurements with positive imaginary components of the complex impedance plane at low frequencies are commonly recognised as an inductive loop. As previously discussed, this inductive loop has been considered a characteristic of systems containing consecutive heterogeneous reactions with potential-dependent adsorbed intermediate species [5,6,7,8]. Ambrosi and Sarli [20] reported that electrochemical reactions that take place within the electrolyte can be governed by both the rate constants and the intermediate species adsorbed on the electrode. The authors reported an electrical circuit representing a faradaic process with adsorption, as shown in Fig. 8. Fig. 8 shows that if intermediate species are involved in the ORR, an additional equivalent network formed by a pseudo-capacitance CPE_{Ad} in parallel with a pseudo-resistance R_{Ad} should be added in series with the former R_C in the R_C-CPE combination that represents simple reaction kinetics. As the adsorption only covers a fraction of the total electrode area, such a fraction fluctuates at the same frequency of the potential but differs in phase with it. Ciureanu and Wang [21] reported the same electrical circuit shown in Fig. 8 to account

for an electrode with adsorbed intermediate species at the interface between dissimilar materials i.e. nafion-carbon in the electrode.

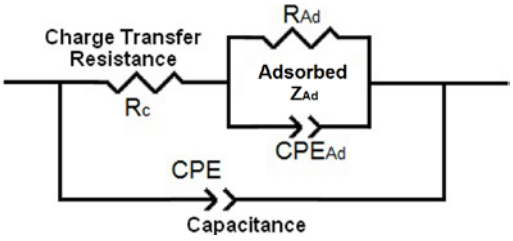

Figure 8. Equivalent electrical circuit representing a faradaic process with adsorption

The second term on the right-hand side of Eq. 1 was derived in previous study [3] by considering simple reaction kinetics $Ox + e^{-} \overset{K}{\leftrightarrow} \mathrm{Re}$ and does not consider adsorbed intermediate species during the ORR which can limit the performance of the PEFC. In Eq. 1 the term expressed as $(R_C + Z_W)$ represents the total process resistance during the ORR, charge transfer resistance R_C in series with mass transport resistance Z_W due to oxygen transport limitations. Bard and Faulkner [22] reported that the overpotential during an electrochemical reaction can be considered as a sum of terms associated with the different reaction steps: mass transport overpotential, charge transfer overpotential and overpotential associated with a preceding reaction. Therefore the electrode reaction can be represented by a resistance composed of a series of resistances representing the various steps during the electrochemical reaction. The term representing the process associated with the adsorbed intermediate species during the ORR Z_{Ad} derived from the circuit in Fig. 8 is connected in series with $(R_C + Z_W)$ in the circuit shown in Fig. 6 to consider the total process resistance during the ORR as reported by Bard and Faulkner [22]. The new electrical circuit for PEFC stack analysis is represented as shown in Fig. 9.

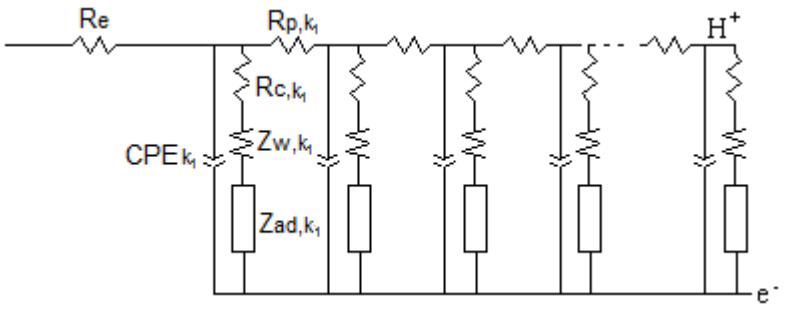

Figure 9. New electrical circuit for PEFC stack analysis

The five elements represented in Fig. 9 are repeated a finite number of times k_N, where k represents a collection of carbon-supported catalytic aggloremates coated by a thin layer of polymer electrolyte. The equation that represents the impedance response of the circuit shown in Fig. 9 can be expressed as:

$$Z_{FC} = R_e + \frac{(R_C + Z_W + Z_{Ad})\gamma \coth(\gamma x)}{1 + Y(i\omega)^P (R_C + Z_W + Z_{Ad})} \qquad [2]$$

where

$$\gamma = \sqrt{R_p \left[\frac{1}{R_C + Z_W + Z_{Ad}} + Y(i\omega)^P \right]} \quad \text{and} \quad Z_{Ad} = \frac{R_{Ad}}{1 + Y_{Ad}(i\omega)^{P_{Ad}} R_{Ad}}$$

The parameters represented in Eq. 2 were fitted to the measured EIS data using the GUI in Matlab®. An increase in the number of parameters in the equation that represents the PEFC impedance response may lead to increased error in the resulting fitting values. Eq. 2 was first fitted to the measured EIS spectra by considering $Z_{Ad} = 0$ and estimating some parameters (R_P, R_C, Y, P, R_e) through a graphical interpretation of the Nyquist plot as shown in Fig. 7. This caused a reduction in the number of parameters to be fitted in the measured EIS data. Secondly, the parameters from Z_{Ad} were fitted to the EIS measurements to reproduce the inductive loop at low frequencies as shown in Fig. 10. The least square error (< 0.1) method was applied.

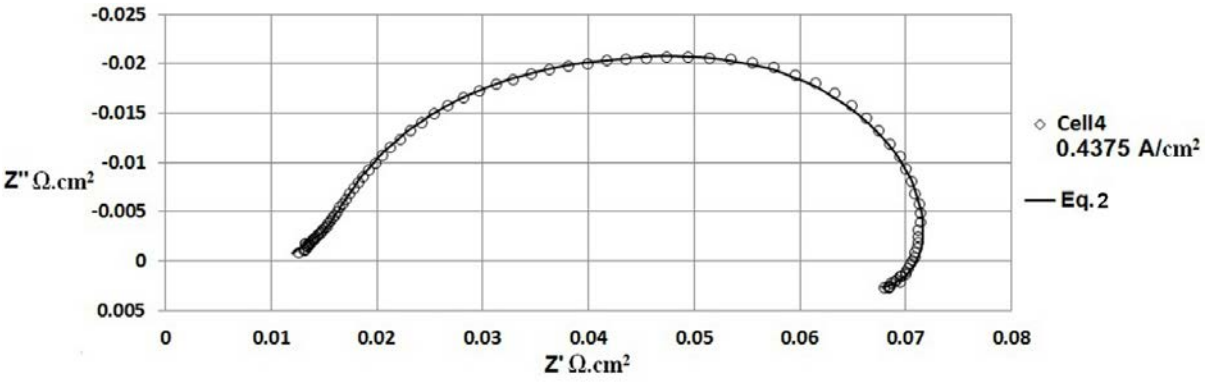

Figure 10. Comparison between measured data and simulated data from Eq. 2

Eq. 1 was derived by considering fundamental electrode theory (Arrhenius equation, Faraday's law, flux of chemical species, exchange current density) in simple reaction kinetics. In this study, Eq. 2 should have been derived as Eq. 1 from fundamental electrode theory considering intermediate species in a two-step ORR. Nevertheless, this approach would result in complicated mathematical equations which could only be solved numerically using mathematical software and only approximate analytical solutions would be delivered. In addition, there may not be assurance that the resulting equation for the PEFC impedance response can be represented through an equivalent electrical circuit. In this study, the electrical circuit reported in a previous study [3] and developed from fundamental electrode theory in simple reaction kinetics as shown in Fig. 6 was combined with the circuit that represents adsorbed intermediate species during the ORR in the CCL as shown in Fig. 8. This methodology simplified the analysis and the resulting electrical circuit can be fitted with real-world EIS measurements to analyse the performance of PEFC stacks.

5. Performance analysis of the Open-Cathode PEFC Stack

This section demonstrates that the new circuit can evaluate the state of health and performance of PEFC cell stacks. The electrical circuit developed in this study can be fitted to EIS results of any H_2/air PEFC stack (low-high power) neglecting contaminants in the anode side and can calculate the

electrochemical and diffusion mechanisms related to the stack performance. For instance, the electrical circuit of this study could be applied with the EIS results of a Ballard's 1.2 kW Nexa^{TM} PEFC stack as reported by Dale *et al.* [4], where a qualitative analysis was reported without attempting to fit an electrical circuit with the EIS results. The new electrical circuit shown in Fig. 9 is fitted to the EIS measurements of the open-cathode stack shown in section 2. The electrochemical and diffusion mechanisms of the measured data of the open-cathode PEFC stack were calculated through Eq. 2 and some parameters are shown in Tab. I.

TABLE I. Charge transfer resistance R_C, mass transport resistance R_W and adsorption resistance R_{Ad} calculated from Eq. 2

	Rc Ω.cm^2	R_w Ω.cm^2	R_{Ad} Ω.cm^2
0.1875A/cm^2			
Cell1	0.7712	0.0128	-0.128
Cell2	0.9312	0.1216	-0.192
Cell3	0.7712	0.1584	-0.176
Cell4	0.7712	0.0736	-0.16
0.3125 A/cm^2			
Cell1	0.6544	0.064	-0.136
Cell2	0.8144	0.176	-0.184
Cell3	0.6544	0.2304	-0.2
Cell4	0.6544	0.152	-0.184
0.4375 A/cm^2			
Cell1	0.6336	0.1952	-0.184
Cell2	0.7568	0.4272	-0.232
Cell3	0.6336	0.504	-0.328
Cell4	0.6336	0.3552	-0.248

Adsorbed species during the ORR. The parameter R_{Ad} that accounts for the adsorbed intermediate species during the ORR resulted in a negative number and became more negative with increasing current density for all cells, as shown in Tab. I. Bai and Conway [23] demonstrated in their work that the inductive loop at low frequencies in electrochemical systems with adsorbed intermediate species is

related to a negative value of adsorbed species coverage φ depending on potential (dφ/dE). Ciureanu and Wang [21] reported EIS measurements in a H_2/ H_2+CO PEFC. EIS measurements showed the inductive loop at low frequencies with increasing bias potential. In their study the electrical circuit shown in Fig. 8 was applied with EIS measurements and this resulted in negative values for R_{Ad}. They concluded that the negative values in R_{Ad} are a result of the decrease of CO coverage on the electrode with increasing bias potential due to oxidation of CO by oxygenated species on the electrode-electrolyte interface. The process responsible for the inductive characteristic at low frequencies shown in Fig. 10 could be attributed to hydrogen crossover through the PEM or bipolar plates to form H_2O_2 during the ORR as reported by Roy *et al.* [6].

Ohmic Resistance. Fig. 11 shows the high frequency region of the EIS measurements at the three different current densities. The measured data of cell 2 are not shown in Fig. 11 as the data of this cell from 10 kHz to 100 Hz showed a different trend compared to the rest of the cells as shown in Figs. 3, 4 and 5. Cell 3 shows a slightly higher ohmic resistance than cell 1 and 4 at the three current densities, this effect can be noticeable in the real part Z' at 10 kHz of the measured data, as shown in Fig. 11. The increase in ohmic resistance could be attributed to dehydration in the PEM which may have been caused by an increase in reaction generated heat in cell 3. Ohmic resistance seems to be more sensitive than charge transfer resistance to the temperature distribution through the stack.

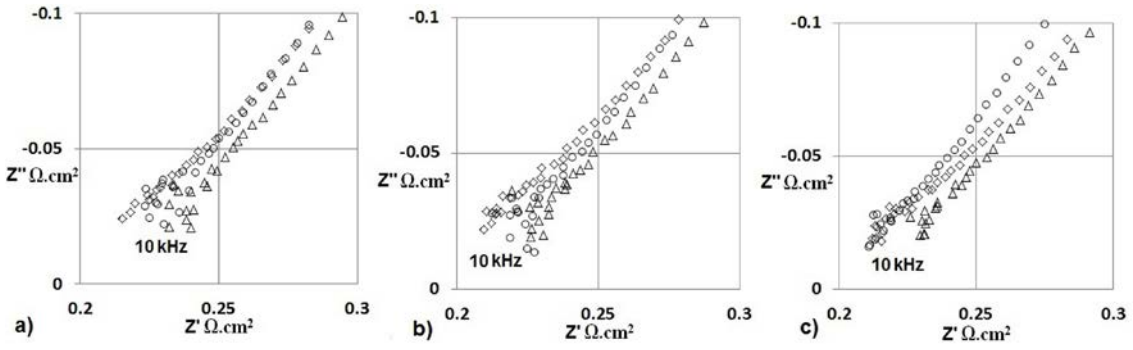

Figure 11. High frequency EIS measurements for cell 1 ◊, cell 3 Δ and cell 4 ○; a) 0.1875A/cm^2, b) 0.3125 A/cm^2, c) 0.4375 A/cm^2

Oxygen Transport Limitations.- The mass transport resistance R_W, due to gaseous oxygen transport limitations and as a function of the gaseous oxygen equilibrium concentration in the CCL-GDL

interface, increases with increasing current density for all cells, as shown in Tab. I. Cells 2 and 3 show higher mass transport resistance than cells 1 and 4. Cell 3 shows the highest mass transport resistance as shown in Fig. 12. The increase in mass transport resistance of cell 3 could be attributed to high water concentration produced by the ORR which affects the transport of oxygen to reach the reaction sites in the CCL; however the increase in ohmic resistance (PEM dehydration) in cell 3, shown in Fig. 9, demonstrates a contrasting case.

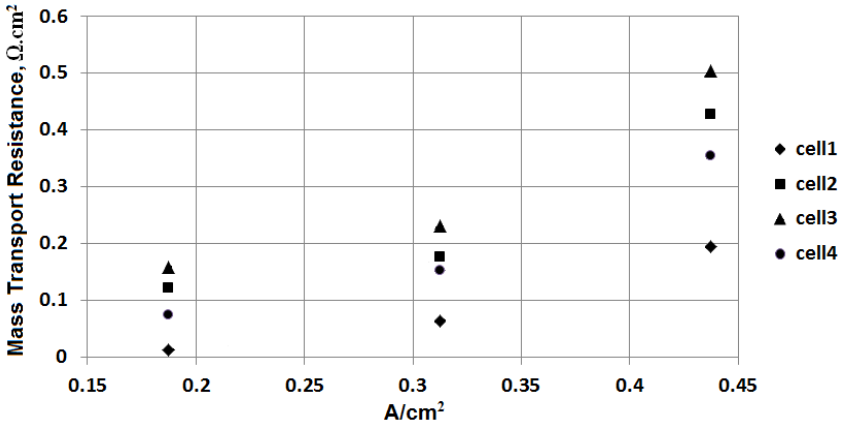

Figure 12. Estimation of mass transport resistance in each individual cell

Santa Rosa *et al.* [24] studied the effect of critical conditions on an open-cathode 8-cell stack operated at ambient temperature and pressure. Three different fans for oxidant supply and cooling were used to investigate how the air flow rate affects the stack performance. A 5 V DC fan was found to be the best option because it ensures enough stack cooling and oxidant supply. The authors concluded that a fan with lower voltage affects the stack performance at medium-high currents because lower air fan flow rate cannot expel excessive reaction generated heat which in turns leads to dehydration in the PEM (high ohmic resistance). In this study, simultaneous EIS measurements demonstrate that inhomogeneity of air flow rate in an open-cathode PEFC stack not only leads to an increase in ohmic resistance but also leads to an increase in oxygen transport limitations in the cells. Limitations in air flow rate decrease the gaseous oxygen equilibrium concentration in the GDL-CCL interface and increase mass transport resistance. The position and distance of the fans with respect to the open cathodes in this particular stack played an important role for oxygen transport limitations. Two 5V DC axial fans were centred 1 cm over the open cathode of cell 3 as shown in Fig. 1a. Air enters the

fan evenly as it follows the physics of moving from a high pressure area into a low pressure area. The air then spreads outwards as it leaves the fan due to a centrifugal force. This results in a vacuum area absent of air flow in the centre of the fan and therefore the majority of the airflow is around the sides of the fan. A fan characteristic curve (FCC) presents three typical regions for axial fans: a stalling, an unstable and an optimal operating region [25]. Sasmito *et al.* [25] reported that the interception between the operating point of an Open-Cathode fuel cell stack and a FCC should be located in the optimal operating region and be sufficiently far away from any unstable and stalling region. With most fans there is no air flow right in the centre of a fan. The majority of the airflow is around the sides of the fan; this effect limits the pressure within the open cathode in cell 3 and thus the operating point of cell 3 corresponds to the stalling point in the FCC. This effect could explain the increase in oxygen transport limitations and the increase in reaction generated heat in cell 3 which increases the ohmic resistance.

Discussion. - The inhomogeneous performance along a PEFC stack can be monitored with the use of simultaneous EIS measurements and an equivalent electrical circuit derived from fundamental electrochemical theory. One of the disadvantages of the EIS technique is that multiple energy controlled processes during the electrochemical reaction can be masked in the impedance measurements. The interpretation of the electrochemical and diffusion mechanisms which are truly happening in a PEFC stack can be unveiled by relating the electrochemical impedance data to an electrical circuit derived from fundamental theory of PEFCs. It is possible to diagnose degradation in MEAs which yield low electrochemical activity in the electrodes through experimental EIS and modelling. Oxygen transport limitations can be diagnosed at low frequencies of EIS measurements. EIS measurements can also provide a direct correlation about variations in air flow through the open cathodes in an open-cathode PEFC. Finally another common effect limiting the stack performance is the presence of adsorbed intermediate species during the ORR. This effect has been identified in EIS measurements as an inductive loop at low frequencies. PEFC stacks are exposed to a range of atmospheric compositions which can include sulphur dioxide, nitrogen oxides, ionic contamination, carbon monoxide, etc. A further investigation to include poisoning effect on PEFC stacks will be

researched in future work. This level of understanding is critical to industry to drive the development, optimisation and running of PEFCs as reliable commercial products.

6. Conclusions

This study has demonstrated that the use of an equivalent circuit derived from electrochemical theory with simultaneous EIS is a powerful tool for in-situ diagnosis of a PEFC stack. EIS measurements that account for each cell in an open-cathode PEFC stack were compared with simulated data from the model reported in the authors' previous study. The model was modified to include adsorbed intermediate species mechanisms during the ORR and the results showed a good agreement between measured data and simulated data. Electrochemical and diffusion mechanisms for each cell in the PEFC stack were calculated through EIS measurements and the model. The results showed that the activation overpotential in the whole PEFC stack is dominated by low electrocatalytic activity in one of the cells. The results also showed that oxygen transport limitations and ohmic resistance are attributed to variations in flow of the air through the open cathodes in the stack. The results also revealed that adsorbed species during the ORR limit the performance of the PEFC stack. This newly established EIS knowledge will enable an assessment of the state of health of operational fuel cell stacks.

Acknowledgments

The authors thank the Mexican National Council for Science and Technology (CONACYT) for the sponsorship of the Ph.D research study of S. Cruz-Manzo (grant no. 183195). The authors also acknowledge Miss. Kathleen McLoughlin for helping with the English Language.

References

[1] R. Mohtadi, W. K. Lee, and J. W. V. Zee, J. Power Sources, 138, 216 (2004).
[2] J. M. Moore, P. L. Adcock, J. B. Lakeman, and G. O. Mopsted, J. Power Sources, 85, 254 (2000).
[3] S. Cruz-Manzo and R. Chen, J. Electroanal. Chem., 694, 45 (2013).
[4] N. V. Dale, M. D. Mann, H. Salehfar, A. M. Dhirde and T. Han, ASME J. Fuel Cell, 7 (2010) 031010/1-031010/10
[5] R. Makharia, M. F. Mathias and D. R. Baker, J. Electrochem. Soc., 152, A970 (2005).
[6] S. K. Roy, M. E. Orazem and B. Tribollet, J. Electrochem. Soc., 154, B1378 (2007).
[7] J. Xie, D. L. Wood III, K. L. More, P. Atanassov, and R. L. Borup, J. Electrochem. Soc., 152, A1011 (2005).
[8] M. Inaba, H. Yamada, J. Tokunaga, and A. Tasaka, Electrochem. Solid-State Lett., 7, A474 (2004).
[9] S. Cruz-Manzo, R. Chen and P. Rama, Int. J. Hydrogen Energy, 38, 1702 (2013).
[10] T. E. Springer, T.A. Zawodzinski, M.S. Wilson, S Gottesfeld, J. Electrochem. Soc. 143 (1996) 587-599.
[11] X. Yan, M. Xou, L. Sun, D. Lian, Q Shen, H. Xu, P. Ming, and B. Yi, Int. J. Hydrogen Energy, 32, 4358 (2007).
[12] S. Asghari, A. Mokmeli, and M. Samavati, Int. J. Hydrogen Energy, 35, 9283 (2010).
[13] N. Wagner, and E. Gülzow, J. Power Sources, 127, (2004) 341–347
[14] V. A. Paganin, C. L. F. Oliveira, E. A. Ticianelli, T. E. Springer and E. R. Gonzalez, Electrochim. Acta, 43, 3761 (1998).
[15] S. Cruz-Manzo, R. Chen and P. Rama, J. Fuel Cell Science Technology, 9, 051002 (2012).
[16] X. Yuan, J. C. Sun, H. Wang and J. Zhang, J. Power Sources, 161, 929 (2006).
[17] N. Fouquet, C. Doulet, C. Nouillant, G. Dauphin-Tanguy and B. Ould-Bouamama, J. Power Sources, 159, 905 (2006).
[18] M. Ciureanu, and R. Roberge, J. of Phys. Chem. B 2001, 105, 3531-3539.
[19] C. H. Hsu, and F. Mansfeld, Corrosion, 57 (2001) 747-748.
[20] V. Ambrosi and A. Di Sarli, Anti-Corrosion, 40, 4 (1993).
[21] M. Ciureanu and H. Wang, J. Electrochem. Soc., 146, 4031 (1999).
[22] A. J. Bard and L. R. Faulkner, Electrochemical Methods, p. 24, John Wiley & Sons Inc., New York (2001).
[23] L. Bai and B. E. Conway, J. Electrochem. Soc., 137, 3737 (1990).
[24] D.T. Santa Rosa, D.G. Pinto, V.S. Silva, R.A. Silva, and C.M. Rangel, Int. J. Hydrogen Energy, 32, 4350 (2007).
[25] P. Sasmito, E. Birgersson, K. W. Lum, A. S. Mujumdar, Renewable Energy, 37, 325 (2012).